Appl. Phys. B 77, 59–63 (2003)
DOI: 10.1007/s00340-003-1247-y

Applied Physics B
Lasers and Optics

D.F. DE SOUSA[1,✉]
L.A.O. NUNES[1]
J.H. ROHLING[2]
M.L. BAESSO[2]

Laser emission at 1077 nm in Nd^{3+}-doped calcium aluminosilicate glass

[1] Instituto de Fisica de Sao Carlos, Universidade de Sao Paulo, P.O. Box 369, 13560-970 Sao Carlos, SP, Brazil
[2] Departamento de Fisica, Universidade Estadual de Maringa, 87020-900 Maringa, PR, Brazil

Received: 18 March 2003/Revised version: 21 May 2003
Published online: 25 July 2003 •

ABSTRACT Laser emission at 1077 nm ($^4F_{3/2} \longrightarrow {}^4I_{11/2}$) was demonstrated in Nd^{3+}-doped low silica content calcium aluminosilicate (LSCA) glass under 810-nm pumping by a Ti:sapphire laser. The slope efficiency of the laser emission was found to be 34% with a 20-mW threshold power. The excited-state absorption (ESA) and stimulated emission were measured between 850 and 1520 nm. The results showed two ESA bands from 931 to 1070 nm ($^4F_{3/2} \longrightarrow {}^2D_{3/2}$, $^2G_{9/2}$, $^4G_{11/2}$, $^2K_{15/2}$) and from 1160 to 1414 nm ($^4F_{3/2}$, $^4G_{9/2} \longrightarrow {}^4G_{7/2}$, $^2K_{13/2}$). The stimulated emission for the laser transition was found to be 45-nm broad with a peak value of 1.8×10^{-20} cm^2. Thermal and mechanical properties of the LSCA glass were compared to the ED-2 and LHG-8 glasses. While the mechanical properties of the LSCA glass are superior to those of the commercial glasses, its temperature coefficient of optical path length is the highest among the three hosts.

PACS 42.60.Pk; 42.70.Ce; 78.66.Jg

1 Introduction

The Nd^{3+}-based laser at around 1064 nm is one of the most studied laser systems due to its high efficiency and large number of applications [1–3]. Although laser action of Nd^{3+} has been demonstrated in several hosts, the search for new solid-state hosts for the Nd^{3+} ion is a continuing task. The host matrix can be either a crystal or a glass and, while a crystal presents higher emission and absorption cross sections, glasses can be produced in larger volumes with adequate optical quality.

Despite the fact that the calcium aluminate system has been known since 1909 [4], properties such as chemical durability and infrared transmission of low silica content or silica-free calcium aluminate glasses were studied only in the 1950s [5, 6]. It is known that the addition of a small amount of silica to the base composition of calcium aluminate increases the glass-forming region, and that melting under vacuum conditions increases the infrared transmission up to 6 μm [7–12]. The effects of rare-earth doping on these glass properties have been explored in the last few years [13–22].

There is a wide variety of Nd-doped laser glasses depending on the composition of the glass network former and modifier ions. Up to now, commercially available high-power glass lasers utilize mainly silicate and phosphate glasses due to their good optical, thermal and mechanical properties. In previous works we have shown that Nd^{3+}-doped low-silica calcium aluminosilicate glass (LSCA) combines a high fluorescence quantum efficiency and excellent mechanical properties, indicating that this glass can be used as an alternative material for the development of Nd^{3+} lasers [16–20]. The motivation to study the LSCA glass is that it provides broader absorption and emission bands without worsening the thermal and mechanical properties. It therefore allows laser action with shorter pulse lengths and at different wavelengths than the 1064 and 1054 nm that are observed in ED-2 and LHG-8 glasses, respectively. In this work we report laser action at 1077 nm of the Nd^{3+}-doped LSCA glass. The doping level was 2 wt. % of Nd_2O_3, or a density of Nd^{3+} ions of about 2×10^{20} cm^{-3}. In [23], a detailed study of the lifetime and Judd–Ofelt calculation for the Nd^{3+}-doped LSCA glass as a function of concentration was performed and it was observed that the sample with 2% of Nd^{3+} showed the maximum emission intensity with high quantum efficiency for the $^4F_{3/2} \longrightarrow {}^4I_{11/2}$ transition.

Figure 1 shows the energy-level diagram of Nd^{3+} in LSCA glass. The shaded areas represent the inhomogeneous broadening of the absorption bands due to the different local fields experienced by the Nd^{3+} ions inside the glass medium along with the thermal broadening. The pump and laser transitions are represented by the thick arrows. The thin downward arrows represent the observed stimulated-emission (SE) transitions and the thin upward arrows indicate the excited-state absorption (ESA) transitions. It is well known that the ESA changes from host to host and the gain properties of a laser medium are strongly affected by this parameter. In [24] the excited-state absorption and stimulated emission of the commercially available glasses LSG-91H (silicate) and LHG-8 (phosphate) were measured in order to quantify the losses due to upconversion in the laser emission of Nd^{3+}. Therefore, the excited state absorption and stimulated emission spectra in the wavelength range from 850 to 1520 nm were also measured in the calcium aluminosilicate glass.

✉ *Current address*: Universität Hamburg, Institut für Laser-Physik, Luruper Chaussee 149, 22761 Hamburg, Germany
Fax: +49-40/8998-5190, E-mail: dsousa@physnet.uni-hamburg.de

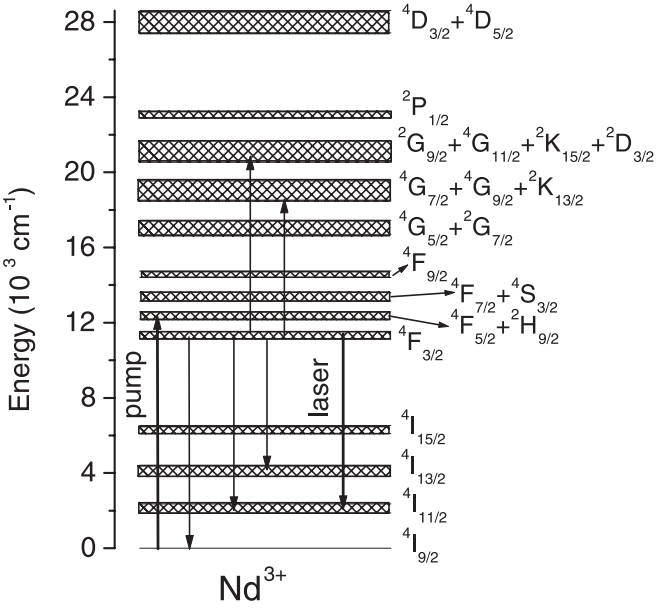

FIGURE 1 Energy-level diagram of Nd^{3+} in LSCA glass

2 Experimental setup

The LSCA glass was prepared from 99.999% purity powders with the following weight (%) composition: 39.5% Al_2O_3, 47.4% CaO, 7% SiO_2, 4.1% MgO and 2% Nd_2O_3. The mixture was melted at 1500 °C in a graphite crucible under vacuum conditions. After 2 h in the melt, the mixture was cooled to room temperature. The obtained sample was cut and polished into a disk of 3-mm thickness and 10-mm diameter for the spectroscopic experiments and into a $3 \times 3 \times 1$-mm^3 block for the laser experiment. The Nd^{3+} concentration is around 2×10^{20} cm^{-3} and it was determined by energy-dispersive X-ray analysis with a digital microscope and the Link Analytical QX2000 software.

For ESA and SE spectra measurements, a pump–probe setup as described in [26] was used to measure the small-signal transmission of the probed sample with and without the presence of the pump beam. The pump beam was from a Ti:sapphire laser operating at 800 nm and the probe beam was from a 200-W tungsten halogen lamp. The pump and probe beams were modulated at 14 and 700 Hz, respectively. The collected signal was dispersed by a 0.3-m Thermo Jarrel Ash monochromator and acquired by a Ge detector. In general, the recorded signal $\Delta I/I$, where I is the transmitted probe intensity and ΔI is the variation in the probe intensity imposed by the pump beam, is given by:

$$\frac{\Delta I}{I} = n_e L A \left[\sigma_{GSA} + \sum_i \frac{n_i}{n_e} (\sigma_{SE} - \sigma_{ESA}) \right], \quad (1)$$

where n_e is the excited population density, n_i/n_e is the fractional excited population density at level i, L is the sample length, A is the amplification factor of the lock-in amplifier, σ_{GSA} is the ground-state absorption cross section and $\sigma_{SE}(i)$ and $\sigma_{ESA}(i)$ are the stimulated-emission and excited-state absorption cross sections of level i, respectively. For Nd^{3+}, the $^4F_{3/2}$ level is the only metastable one, which leads to $n_i/n_e = 1$ and (1) can be rewritten as:

$$\frac{\Delta I}{I} = n_e L A \left[\sigma_{GSA} + \sigma_{SE} - \sigma_{ESA} \right]. \quad (2)$$

The calibration of the $\Delta I/I$ spectrum is usually done by choosing a wavelength at which only ground-state absorption exists. In this case, the expression for $\Delta I/I$ reduces to:

$$\frac{\Delta I}{I} = n_e L A \sigma_{GSA}. \quad (3)$$

The ground-state absorption transition is measured at the pump–probe setup and compared to the ground-state absorption cross section obtained at a commercial spectrophotometer to obtain the factor $n_e LA$. The $\sigma_{SE} - \sigma_{ESA}$ spectrum is obtained by subtracting the ground-state absorption cross section from $\sigma_{GSA} + \sigma_{SE} - \sigma_{ESA}$.

The laser experiment was performed with an end-pumped resonator. The rear mirror was plane with a transmission coefficient of 90% for the pump wavelength and a reflection coefficient of 100% for the laser wavelength. The output mirror had a 50-mm curvature radius with a transmission coefficient of 3% at the laser wavelength. The sample length was 1 mm.

3 Results

Figure 2 shows the $\Delta I/I$ spectrum of the Nd^{3+}-doped LSCA glass. The observed spectrum is similar to the results published by Adam et al. [25] for Nd^{3+} in fluoride glasses apart from the red shift of the absorption and emission bands due to the nepheulaxetic effect that is stronger in the oxide glass. For the calibration procedure, the σ_{GSA} of the $^4I_{9/2} \longrightarrow {}^4F_{3/2}$ transition measured in a Perkin–Elmer Lambda 900 spectrophotometer was summed with the σ_{SE} of the $^4F_{3/2} \longrightarrow {}^4I_{9/2}$ transition obtained by the Füchtbauer–Ladenburg (F–L) expression:

$$\frac{\beta_{i-j}}{\tau_i} = \frac{8n^2\pi}{c^2} \int \nu^2 \sigma_{em}(\nu)\, d\nu, \quad (4)$$

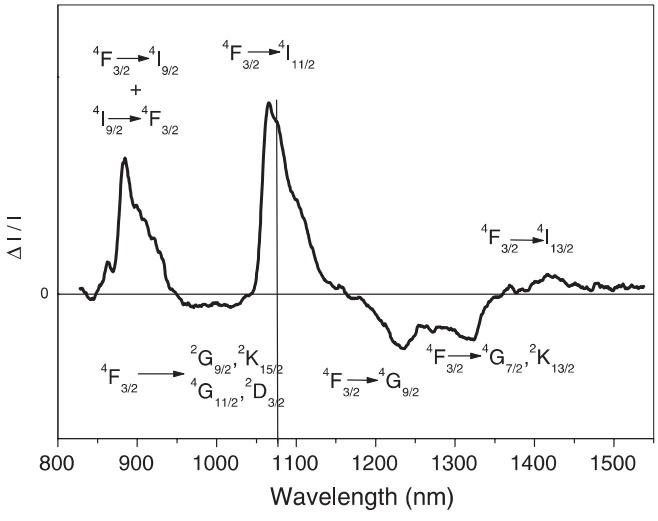

FIGURE 2 $\Delta I/I$ spectrum of the Nd^{3+}-doped LSCA glass. The *vertical line* indicates the wavelength of the laser emission

where the branching ratio of the $i-j$ transition (β_{i-j}) and the radiative lifetime of level i (τ_i) were obtained by Judd–Ofelt calculation [27, 28]. n is the refractive index of the medium, c is the velocity of light, ν is the frequency and σ_{em} is the emission cross section. The summed curve was compared to the measured curve at the pump–probe experiment in order to obtain the factor $n_e LA$. This was possible because no ESA is expected at the short-wavelength side of this band.

The measured $\Delta I/I$ spectrum was then divided by $n_e LA$ to obtain the cross-section scale. The accuracy of our emission cross section depends on the precise determination of the product $n_e LA$. Considering that the F–L expression can generate an error of at least 10% in the emission cross section (mainly due to the uncertainties in the Judd–Ofelt calculations), we expect that the accuracy of the SE spectrum is also not better than 10% around the measured value. On the other hand, the ESA spectrum in the same spectral range has a larger error due to its lower intensity. The vertical line in Fig. 2 indicates the wavelength of the observed laser emission. The two ESA bands from 931 to 1070 nm and from 1160 to 1414 nm are due to the $^4F_{3/2} \longrightarrow {}^2D_{3/2}$, $^2G_{9/2}$, $^4G_{11/2}$, $^2K_{15/2}$ and $^4F_{3/2} \longrightarrow {}^4G_{9/2}$, $^4G_{7/2}$, $^2K_{13/2}$ transitions, respectively. As observed by Adam et al. [25], the ESA transitions $^4F_{3/2} \longrightarrow {}^4G_{9/2}$, $^4G_{7/2}$, $^2K_{13/2}$ around 1300 nm prevent laser action on the $^4F_{3/2} \longrightarrow {}^4I_{13/2}$ transition.

Figure 3 shows the $\sigma_{SE} - \sigma_{ESA}$ spectrum (dashed line), obtained by subtracting the ground-state absorption $^4I_{9/2} \longrightarrow {}^4F_{3/2}$ from the calibrated $\Delta I/I$ spectrum, along with the σ_{ESA} spectrum (solid line), obtained by subtracting the σ_{SE} bands $^4F_{3/2} \longrightarrow {}^4I_{9/2}$, $^4F_{3/2} \longrightarrow {}^4I_{11/2}$ and $^4F_{3/2} \longrightarrow {}^4I_{13/2}$, which were calculated by the F–L expression. The branching ratios and lifetimes used in the F–L expression were again obtained by the Judd–Ofelt theory. The laser wavelength is indicated by the vertical line. The cross section for the stimulated-emission $^4F_{3/2} \longrightarrow {}^4I_{11/2}$ transition is comparable to the glasses measured in [24, 25]. The ESA transitions observed in the LSCA glass are broader and present almost the same intensity as the fluoride glasses [25] and the peak of the stimulated-emission cross section for the $^4F_{3/2} \longrightarrow {}^4I_{13/2}$ transition is about 12% higher than the one measured for the silicate glass LSG-91H [24]. Nevertheless, the Nd^{3+}-doped LSCA glass presents a broader emission bandwidth than the silicate. Such a result indicates that the upconversion losses by energy transfer are not negligible in the LSCA glass as well as in the silicate LSG-91H and phosphate LHG-8. Figure 4 shows the measured laser power plotted against absorbed power. A threshold power of 20 mW and a slope efficiency of 34% were observed for Nd^{3+} in LSCA glass.

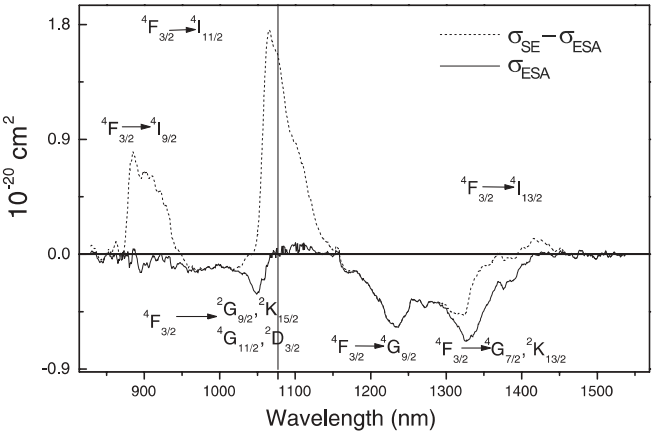

FIGURE 3 $\sigma_{SE} - \sigma_{ESA}$ (*dashed line*) and σ_{ESA} (*solid line*) spectra of the Nd^{3+}-doped LSCA glass

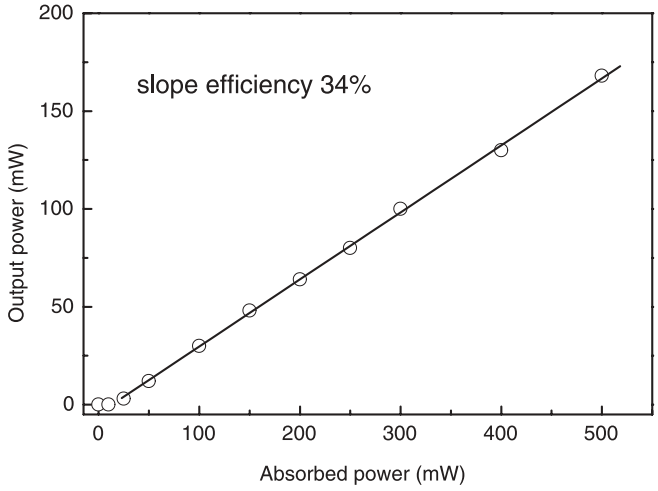

FIGURE 4 Measured threshold and slope efficiency of the Nd^{3+}-doped LSCA glass laser oscillator

4 Discussion

The small-signal gain profile of the $^4F_{3/2} \longrightarrow {}^4I_{11/2}$ transition can be obtained by means of the expression:

$$G(\lambda) = n\,(^4F_{3/2})\,\sigma_{SE} - n\,(^4F_{3/2})\,\sigma_{ESA1} - n\,(^4I_{11/2})\,\sigma_{ESA2}\,, \tag{5}$$

where $n(i)$ is the population density of level i, σ_{SE} is the $^4F_{3/2} \longrightarrow {}^4I_{11/2}$ emission cross section and σ_{ESA1} and σ_{ESA2} are the $^4F_{3/2} \longrightarrow {}^2G_{9/2}$, $^2K_{15/2}$, $^4G_{11/2}$, $^2D_{3/2}$ and $^4I_{11/2} \longrightarrow {}^4F_{3/2}$ excited-state absorption cross sections, respectively. As the $^4I_{11/2}$ level energy is about 1881 cm^{-1}, its excitation density calculated by the Boltzmann population factor is found to be about $1.2 \times 10^{-4} n\,(^4I_{9/2})$. Such a density can be neglected in the low signal gain calculation and we have a simplified form for (5):

$$G(\lambda) = n\,(^4F_{3/2})\,\sigma_{SE} - n\,(^4F_{3/2})\,\sigma_{ESA1}\,. \tag{6}$$

In this situation the gain profile can be obtained directly from the spectrum in Fig. 3 multiplied by the population of the $^4F_{3/2}$ level. The σ_{ESA} spectrum in Fig. 3 shows that the excited-state absorption $^4F_{3/2} \longrightarrow {}^2G_{9/2}$, $^2K_{15/2}$, $^4G_{11/2}$, $^2D_{3/2}$ extends to 1070 nm but does not cause a significant loss to the $^4F_{3/2} \longrightarrow {}^4I_{11/2}$ emission band.

Table 1 compares the laser performance under continuous-wave pumping of the Nd^{3+}:LSCA obtained in this work with the commercially available Nd^{3+}-doped LHG-5 glass reported in [29]. λ_{laser} (λ_{pump}) is the laser (pump) wavelength, η_s is the slope efficiency, P_{th} is the threshold power, T is the transmission of the output mirror at the laser wavelength and L is the sample length. For an end-pumped laser, the slope

Property	LHG-5	LSCA
λ_{laser}	1054 nm	1077 nm
λ_{pump}	802 nm	810 nm
η_s	42%	34%
P_{th}	12.2 mW	20 mW
T	0.4%	3%
L	2 mm	1 mm

TABLE 1 Performance of the lasers obtained from Nd^{3+}-doped LHG-5 [29] and LSCA glasses

efficiency is given by [30]:

$$\eta_s = F_p \frac{T}{l} \frac{h\nu_{laser}}{h\nu_{pump}}, \quad (7)$$

where F_p is the fraction of pump power absorbed in the active region, l is the total round-trip loss including the output coupling T, h is the Planck constant and ν_{laser} (ν_{pump}) is the laser (pump) frequency. In the expression for η_s the only unknown parameters are F_p and l, so the ratio F_p/l was calculated from the measured slope of the two lasers, giving the results 15 and 139 for the LSCA and LHG-5, respectively. This means that in the best possible case of 100% pump absorption ($F_p = 1$) the maximum cavity losses are 0.0667 for the LSCA laser and 0.0072 for the LHG-5 laser. The $l/2L$ quantity, where L is the rod length, is then given by $0.0018\,mm^{-1}$ and $0.0333\,mm^{-1}$ for the LHG-5 and LSCA lasers, respectively. Although this comparison needs the assumption that $F_p = 1$, it indicates that the scattering losses in the LSCA glass are still high and need to be reduced by modifying the sample preparation. Reducing the scattering losses will also improve the threshold pump power.

Now it is interesting to compare other parameters of commercially available Nd^{3+} laser glasses to those of Nd^{3+}:LSCA. Table 2 lists optical, mechanical and thermal properties of the commercially available Nd^{3+} laser glasses LHG-8 and ED-2 along with the ZBAN, tellurite and LSCA glasses. The longer radiative lifetime of the $^4F_{3/2}$ level in ZBAN glass is mainly due to the lower phonon energy of this glass compared to other matrices, while the remarkably short lifetime in tellurite glass is a common fact in chalcogenide hosts and can be attributed to the high refractive index of the matrix and high covalence in bonding, which lead to a higher radiative-transition probability. The large amount of Al_2O_3 in the LSCA glass leads to broader emission bandwidths ($\Delta\lambda$) [1] and, consequently, lower emission cross sections. On the other hand, this large bandwidth permits the achievement of pulsed laser action with short pulse length. The theoretical limit for the pulse length is approximatively given by the inverse of the gain line width $1/\Delta\nu$. Using the results of Table 2, the minimum pulse length for the LHG-5 is approximately 0.2 ps while the LSCA glass can achieve 0.08 ps. The large-gain line width also permits laser action at longer wavelengths than can be achieved in the phosphates LHG-8 and LHG-5 and in the silicate ED-2 glasses. A laser experiment with a slightly different output mirror ($T = 5\%$) showed laser action of LSCA glass at 1090 nm with a threshold power of 50 mW and a slope efficiency of 30%.

The hardness (H) of the LSCA glass is 2.6 and 1.4 times higher than that of LHG-8 and ED-2 glasses, respectively. This feature improves the Young modulus (E) and the fracture toughness (K_{IC}) of the LSCA glass compared to the LHG-8 and ED-2 matrices. The Young modulus is 50 GPa, 90 GPa and 110 GPa for LHG-8 [2], ED-2 [2] and LSCA [18, 31], respectively, while the fracture toughness is found to be $0.46\,MPa\,m^{1/2}$, $0.83\,MPa\,m^{1/2}$ and $1.4\,MPa\,m^{1/2}$ in the same order. Using the above-mentioned properties, the thermal shock resistance (R_s) can be calculated with the expression:

$$R_s = \frac{k(1-\mu)K_{IC}}{E\alpha}, \quad (8)$$

where k is the thermal conductivity, μ is Poisson's ratio and α is the thermal expansion coefficient. The R_s parameters for LHG-8, ED-2 and LSCA glasses are respectively $0.32\,W\,m^{-1/2}$, $1.02\,W\,m^{-1/2}$ and $1.72\,W\,m^{-1/2}$. This is an important figure of merit for high-power lasers that relates thermal and mechanical properties to the maximum thermal load the glass can be subjected to without failure.

Another important thermal–optical property is the temperature coefficient of the optical path length (δ) that accounts for the optical distortion in the laser beam by changing the optical path length. The lower δ, the smaller the optical path change with increasing temperature. The expression for δ is given by:

$$\delta = \frac{dn}{dT} + (n-1)\alpha, \quad (9)$$

Property	LHG-8 [2]	ED-2 [2]	ZBAN [32]	Tellurite [33]	LSCA [16, 23, 31]
τ_r (μs)	315	310	419	170	310
λ_{laser} (nm)	1054	1064	1048	1066	1077
σ_{em} (10^{-20} cm^2)	4.2	2.7	3.2	3.9	1.8
n(589.3 nm)	1.5612	1.5672	–	1.8–2.3	1.67
$\Delta\lambda$ (nm)	20.1	27.8	30.5	26	45
ϱ (g cm^{-3})	2.83	2.54	–	–	2.94
H (GPa)	3.21	5.876	–	–	8.5
μ	0.26	0.24	–	–	0.29
c_p (J g^{-1} K^{-1})	0.75	0.92	–	–	0.93
k (W m^{-1} K^{-1})	0.52	1.35	–	–	1.56
D (10^{-7} m^2 s^{-1})	2.4	5.8	–	–	5.7
α (10^{-6} K^{-1})	11.2	9.2	–	–	8.2
dn/dT (10^{-6} K^{-1})	−5.3	2.9	–	–	8.0

TABLE 2 Comparison between the optical, thermal and mechanical properties of the LSCA glass and the commercially available LHG-8 from Hoya and ED-2 from Schott. The ZBAN and tellurite glasses are also included. τ_r is the radiative lifetime of the $^4F_{3/2}$ level measured in a low-concentration sample, λ_{laser} is the wavelength of the laser emission, σ_{em} is the emission cross section of the laser emission, n is the refractive index, $\Delta\lambda$ is the full width at half maximum (FWHM) of the fluorescence line, ϱ is the density of the glass, H is the hardness, μ is Poisson's ratio, c_p is the specific heat, k is the thermal conductivity, D is the thermal diffusivity, α is the thermal expansion coefficient and dn/dT is the temperature coefficient of the refractive index

where n is the refractive index and dn/dT is the temperature change in refractive index. Using the reported values for dn/dT in LHG-8 [2], ED-2 [2] and LSCA [16] glasses, δ can be calculated as $0.6 \times 10^{-6}\,K^{-1}$, $8 \times 10^{-6}\,K^{-1}$ and $13.5 \times 10^{-6}\,K^{-1}$. The LHG-8 glass presents a low δ because its dn/dT is negative (Table 2) and the high δ of the LSCA glass is attributed to its large dn/dT.

From the above statements one can say that while the scattering loss problem is not solved, the LSCA glass is still not better than the commercial counterparts concerning the compromise between thermal/mechanical properties and optical performance for high-power lasers. On the other hand, the LSCA glass presents a broader emission band and allows laser emission at different wavelengths than the ones observed with the silicate and phosphate glasses. Furthermore, the broad emission band can be used to obtain pulsed operation with less than 1 ps of pulse length. From this point of view, the LSCA glass is a potential candidate for a new Nd^{3+} laser host and more effort must be employed to reduce the scattering losses.

5 Conclusions

Laser and excited-state absorption experiments were performed with a Nd^{3+}-doped LSCA glass. The laser emission was centered at 1077 nm with a slope efficiency of 34% and a threshold power of 20 mW. This is comparable to, but not better than, the commercial glass LHG-5, due to the high scattering loss found in the LSCA glass. On the other hand, the mechanical properties of the LSCA glass are superior to those of the commercially available materials, and the studied glass presents a thermal shock resistance which is 5.4 times greater than that of the LHG-8 glass and 1.7 times greater than that of the ED-2 glass. Concerning the change of the optical path with increasing temperature, the situation is inverted due to the high dn/dT of the LSCA glass compared to the commercially available glasses. These results indicate that LSCA is a promising Nd^{3+} laser material for 1077 nm. To achieve a competitive device with higher efficiency, further improvement in the LSCA base composition and sample preparation are needed, in order to decrease both the scattering losses and the temperature coefficient of the optical path length. The ESA data showed two excited-state absorption bands at 1000 and 1300 nm, respectively. The first-mentioned absorption band causes minimal excited-state absorption loss for the $^4F_{3/2} \longrightarrow {}^4I_{11/2}$ emission up to 1070 nm, while both bands contribute to the losses by energy-transfer upconversion [24].

REFERENCES

1 J.H. Campbell, T.I. Suratwala: J. Non-Cryst. Solids **263–264**, 318 (2000)
2 C.F. Rapp: In *Laser Glasses – Handbook of Laser Science and Technology*, Vol. V (CRC, Boca Raton, FL 1987) p. 339
3 S.E. Stokowski: In *Glass Lasers – Handbook of Laser Science and Technology,* Vol. I (CRC, Boca Raton, FL 1982) p. 215
4 E.S. Shepherd, G.A. Rankin, F.E. Wright: Am. J. Sci. **28**, 293 (1909)
5 J.M. Florence, F.W. Glae, M.H. Black: J. Res. Nat. Bur. Stand. **55**, 231 (1955)
6 H.C. Hafner, N.J. Kreidl, R.A. Weidel: J. Am. Ceram. Soc. **41**, 315 (1958)
7 J.R. Dawy: Glass Technol. **19**, 32 (1978)
8 G.Y. Onoda, S.D. Brown: J. Am. Ceram. Soc. **53**, 311 (1970)
9 J.E. Shelby: J. Am. Ceram. Soc. **68**, 155 (1985)
10 P.L. Higby, R.J. Ginther, I.D. Aggarwal, E.J. Friebele: J. Non-Cryst. Solids **126**, 209 (1990)
11 W.A. King, J.E. Shelby: Phys. Chem. Glasses **37**, 1 (1996)
12 J.E. Shelby, C.M. Shaw, M.S. Spess: J. Appl. Phys. **66**, 1149 (1989)
13 E.V. Uhlmann, M.C. Weinberg, N.J. Kreidl, L.L. Burgner, R. Zanoni, K.H. Church: J. Non-Cryst. Solids **178**, 15 (1994)
14 D.F. de Sousa, L.F.C. Zonetti, M.J.V. Bell, J.A. Sampaio, L.A.O. Nunes, M.L. Baesso, A.C. Bento, L.C.M. Miranda: Appl. Phys. Lett. **47**, 908 (1999)
15 M.L. Baesso, A.C. Bento, L.C.M. Miranda, D.F. de Sousa, J.A. Sampaio, L.A.O. Nunes: J. Non-Cryst. Solids **276**, 8 (2000) and references therein
16 M.L. Baesso, A.C. Bento, A.A. Andrade, T. Catunda, J.A. Sampaio, S. Gama: J. Non-Cryst. Solids **219**, 165 (1997)
17 M.L. Baesso, A.C. Bento, A.A. Andrade, J.A. Sampaio, E. Pecoraro, L.A.O. Nunes, T. Catunda, S. Gama: Phys. Rev. B **57**, 10 545 (1998)
18 M.L. Baesso, A.C. Bento, A.R. Duarte, A.M. Neto, L.C.M. Miranda, J.A. Sampaio, T. Catunda, S. Gama, F.C.G. Gandra: J. Appl. Phys. **85**, 8112 (1999)
19 J.A. Sampaio, T. Catunda, F.C.G. Gandra, S. Gama, A.C. Bento, L.C.M. Miranda, M.L. Baesso: J. Non-Cryst. Solids **247**, 196 (1999)
20 S.M. Lima, J.A. Sampaio, T. Catunda, A.C. Bento, L.C.M. Miranda, M.L. Baesso: J. Non-Cryst. Solids **273**, 215 (2000)
21 D.F. de Sousa, L.F.C. Zonetti, M.J.V. Bell, J.A. Sampaio, L.A.O. Nunes, M.L. Baesso, A.C. Bento, L.C.M. Miranda: Phys. Rev. B **62**, 3176 (2000)
22 J.A. Sampaio, T. Catunda, S. Gama, M.L. Baesso: J. Non-Cryst. Solids **284**, 210 (2001)
23 E. Pecoraro, J.A. Sampaio, L.A.O. Nunes, S. Gama, M.L. Baesso: J. Non-Cryst. Solids **277**, 73 (2000)
24 J.L. Doualan, C. Maunier, D. Descamps, J. Landais, R. Moncorgé: Phys. Rev. B **62**, 4459 (2000)
25 J.L. Adam, J.L. Doualan, L. Griscom, S. Girard, R. Moncorgé: J. Non-Cryst. Solids **256–257**, 276 (1999)
26 J. Koetke, G. Huber: Appl. Phys. B **61**, 151 (1995)
27 B.R. Judd: Phys. Rev. **127**, 750 (1962)
28 G.S. Ofelt: J. Chem. Phys. **37**, 511 (1962)
29 W.J. Kozlowsky, T.Y. Fan, R.L. Byer: Opt. Lett. **11**, 788 (1986)
30 M.J.F. Digonnet, C.J. Gaeta: Appl. Opt. **24**, 333 (1985)
31 J.A. Sampaio, M.L. Baesso, S. Gama, A.A. Coelho, J.A. Eiras, I.A. Santos: J. Non-Cryst. Solids **304**, 293 (2002)
32 R.R. Petrin, M.L. Kliewer, J.T. Beasley, R.C. Powell, I.D. Aggarwal, R.C. Ginther: IEEE J. Quantum Electron. **QE-27**, 1031 (1991)
33 N. Lei, B. Xu, Z. Jiang: Opt. Commun. **127**, 263 (1996)